Photoionization studies of C_2H_5I and C_6H_6 perturbed by Ar and SF_6

C. M. Evans [a,b], J. D. Scott [a,b], F. H. Watson [a], G. L. Findley [a,*]

[a] *Department of Chemistry, University of Louisiana at Monroe, Monroe, LA 71209, USA*
[b] *Center for Advanced Microstructures and Devices (CAMD) and Department of Chemistry, Louisiana State University, Baton Rouge, LA 70803 USA*

submitted 20 April 2000

Abstract

We present photoionization spectra of C_2H_5I and C_6H_6 doped into Ar and SF_6, and photoabsorption spectra of C_2H_5I doped into Ar. The observation of subthreshold photoionization in C_2H_5I/SF_6 and C_6H_6/SF_6 is discussed in terms of dopant (D)/perturber (P) interactions involving the excited state processes of $D^* + P \rightarrow D^+ + P^-$ and $D^* + P \rightarrow [DP]^+ + e^-$, where D^* is a discrete Rydberg state of the dopant. The density-dependent energy shifts of high-n Rydberg states observed in the subthreshold photoionization spectra are used to obtain the zero-kinetic-energy electron scattering length for SF_6. Similarly, the zero-kinetic-energy electron scattering length of Ar obtained from the density-dependent energy shifts of C_2H_5I Rydberg states is presented. (Electron scattering lengths obtained here for SF_6 and Ar accord with values previously obtained using the density-dependent energy shifts of high-n Rydberg states of CH_3I doped into these two perturber gases.)

1. Introduction

Numerous photoabsorption [1-5], photoionization [2,6-15] and field ionization [16] studies of dopant/perturber (D/P) systems have exploited perturber pressure effects on molecular dopant Rydberg state energies and ionization energies as a means of measuring electron scattering lengths in the perturber medium. In many of these systems [2,8,10-12,14,15], photoionization structure has been observed to occur at energies lower than the unperturbed dopant ionization threshold. This subthreshold photoionization structure, which tracks the photoabsorption of discrete dopant Rydberg states in the same energy region, has been used [8,10,14] in the evaluation of perturber pressure effects necessary for the extraction of electron scattering lengths. The nature of those processes leading to subthreshold photoionization is not well understood, however.

Subthreshold photoionization has traditionally been explained as resulting from the collisional transfer of translational, rotational or vibrational energy from a perturber to an excited-state dopant [6]. However, photoionization spectra of CH_3I [11,12,14] and of CH_3I doped into Xe [10], Ar [2,15], CO_2 [8,15], N_2 [15] and SF_6 [14] exhibit rich subthreshold structure beginning 0.17 eV below the CH_3I ionization limit, which is much too low an onset to be accounted for by collisional transfer of perturber translational energy to an excited-state dopant molecule. Moreover, the observation of similar subthreshold spectra in systems containing both atomic and molecular perturbers apparently excludes rotational and vibrational energy transfer as potential mechanisms as well. (Vibrational autoionization, however, has been found to give rise to a weak subthreshold structure in CH_3I at very low perturber pressures [11,12,17]. At

*Corresponding author. E-mail: chfindley@ulm.edu

higher perturber pressures, this vibrational autoionization is supplanted by a subthreshold structure having a much lower energy onset [11,12,14].) Finally, CH_3I photochemistry has been ruled out on the basis of energetics in these systems by Ivanov and Vilesov [11,12]. It becomes important, then, to study subthreshold photoionization as a function of temperature, dopant number density and perturber number density in order to explore the nature of those mechanisms leading to subthreshold structure.

We recently measured subthreshold photoionization of CH_3I doped into Ar, N_2, CO_2 [15] and SF_6 [14]. In the absence of any temperature effect indicative of vibrational autoionization, we proposed two possible pathways leading to subthreshold structure [14,15]. The first pathway requires direct dopant/perturber interactions leading both to charge transfer and to dimer ion formation [14]:

$$D^* + P \rightarrow D^+ + P^- \quad (1)$$

$$\rightarrow [DP]^+ + e^- , \quad (2)$$

where D^* is a Rydberg state of the dopant molecule. Since the first process [i.e., eq. (1)] of this pathway invokes electron attachment to the perturber, this mechanism should be enhanced in perturbers exhibiting a large electron attachment cross-section. The second process [i.e., eq. (2)] constitutes associative ionization, which should lead to a perturber-dependent onset energy as a result of dopant/perturber dimerization.

The second pathway, namely [15],

$$D^* + D \rightarrow D^+ + D^- \quad (3)$$

$$D^* + D + P \rightarrow D_2^+ + P + e^- , \quad (4)$$

differs significantly with regard to dopant/perturber interactions. In the first process [i.e., eq. (3)] of this pathway, electron attachment is now to the dopant rather than to the perturber. Therefore, if the dopant itself has a large enough electron attachment cross-section, subthreshold structure should be observed even when the perturber has a low electron attachment cross-section. In the second process [i.e., eq. (4)], since the associative ionization is now only stabilized by the perturber [18], the onset energy should remain constant even if the perturber is varied.

For either of the above pathways, the subthreshold photocurrent will be given by a sum of two contributions, namely [14,15],

$$i = i_{ea} + i_{ai} , \quad (5)$$

where i_{ea} is the photocurrent contribution resulting from electron attachment, and i_{ai} is the photocurrent contribution resulting from associative ionization. In pathway 1, the electron attachment contribution i_{ea} is given by [cf. eq. (1)]

$$i_{ea} = k_1^{(1)} \rho_{D^*} \rho_P , \quad (6)$$

while in pathway 2 this contribution is given by [cf. eq. (3)]

$$i_{ea} = k_1^{(2)} \rho_{D^*} \rho_D . \quad (7)$$

In eqs. (6, 7), $k_1^{(1,2)}$ is the effective rate constant for the electron attachment process, and ρ_A is the number density of species A. If we now assume that the electron attachment is *saturated* (i.e., dependent only upon ρ_{D^*}), and if we further assume that $\rho_{D^*} \propto \rho_D$ in the linear absorption regime, eqs. (6,7) both reduce to [14,15]

$$i_{ea} = k_1 \rho_D , \quad (8)$$

where k_1 is an empirical rate constant for saturated electron attachment. Under these assumptions, then, the electron attachment contribution to the total subthreshold photocurrent has the same form for both pathways 1 and 2.

Pathways 1 and 2 differ with regard to the associative ionization contribution to the subthreshold photocurrent, however. If we again assume that $\rho_{D^*} \propto \rho_D$ in the linear absorption regime, the associative ionization contribution from pathway 1 [cf. eq. (2)] is given by [14]

$$i_{ai} = k_2^{(1)} \rho_D \rho_P , \quad (9)$$

while the same contribution from pathway 2 [cf.

eq. (4)] is given by [15]

$$i_{ai} = k_2^{(2)} \rho_D^2 \rho_P \ , \qquad (10)$$

where $k_2^{(1,2)}$ is the effective rate constant for associative ionization.

By combining eqs. (8-10) and by replacing $k_2^{(1,2)}$ with an empirical associative ionization rate constant k_2, we find that the total subthreshold photocurrent is

$$i = (k_1 + k_2 \rho_P) \rho_D \qquad (11)$$

for pathway 1, and

$$i = (k_1 + k_2 \rho_P \rho_D) \rho_D \qquad (12)$$

for pathway 2. Clearly, when a dopant/perturber system exhibits subthreshold photoionization, both pathways 1 and 2 may be operative simultaneously. However, in a system where both pathways are available [cf. eqs. (1,3) and eqs. (2,4)], pathway 1 will dominate when $\rho_P >> \rho_D$. Therefore, if the perturber has a large electron attachment cross-section, one should expect that the subthreshold photocurrent will be modeled by eq. (11), with little contribution from pathway 2. We have indeed shown this to be the case for a constant number density of CH_3I doped into varying number densities of SF_6 [14]. Moreover, we have also shown [14] that eq. (11) holds for the degenerate case (D = P = CH_3I) of varying number densities of pure CH_3I, in which eq. (1) of pathway 1 is identical to eq. (3) of pathway 2.

If the perturber has a small electron attachment cross-section, one should expect that the subthreshold photocurrent will be modeled by eq. (12), with little contribution from pathway 1. In fact, we have indeed found that eq. (12) is sufficient to explain the subthreshold photocurrent of a constant number density of CH_3I doped into varying number densities of Ar, N_2 and CO_2 [15].

Since k_1 is proportional to the (saturated) electron attachment cross-section which, in turn, scales as the principal quantum number n of the dopant Rydberg state [6], k_1 should vary linearly with n. k_2, on the other hand, is determined by molecular interactions which are dependent upon the excited state polarizability of the dopant molecule [19]. Since Rydberg state polarizability scales as n^7 [6], k_2 should also scale as n^7. We have shown that the n and n^7 scaling of k_1 and k_2, respectively, holds for pure CH_3I [14] , as well as for the CH_3I/P systems with P = Ar, N_2, CO_2 [15] and SF_6 [14]. Therefore, the processes of electron attachment [i.e., eqs. (1, 3)] and associative ionization [i.e., eqs. (2, 4)] are sufficient to explain the density dependence and n dependence of the observed subthreshold photoionization structure. (We should note, however, that other mechanisms can not positively be ruled out, provided that such mechanisms scale as n (and are saturated) or as n^7.)

As mentioned above, we have observed [14] subthreshold photoionization structure in pure CH_3I that is quadratically dependent on CH_3I number density, and that can be modeled within pathway 1 [i.e., eqs. (1,2)] by setting P = D = CH_3I. We have also observed subthreshold photoionization structure in CH_3I/SF_6 that is linearly dependent on the SF_6 number density [14]. This CH_3I/SF_6 subthreshold structure was explained within pathway 1, since SF_6 has a large electron attachment cross-section [6,20]. However, the existence of subthreshold structure in pure CH_3I implies that, in the presence of a perturber with a small electron attachment cross-section, subthreshold photoionization of CH_3I can proceed through pathway 2 [i.e., eqs. (3, 4)]. The availability of pathway 2 was also indicated by the presence of subthreshold photoionization for CH_3I doped into Ar, N_2 and CO_2 [15] which was linearly dependent upon the perturber number density at constant CH_3I pressure. (Subthreshold photoionization structure has also been observed in HI [21]. However, this structure has not been studied in detail due to the complexity of the observed subthreshold current.) Additional studies involving different dopant molecules are needed in order to develop a better understanding of those properties necessary for a dopant/perturber

system to exhibit subthreshold photoionization, and to probe the general applicability of pathway 1 [i.e., eqs. (1, 2)] and pathway 2 [i.e., eqs. (3, 4)].

In the present Paper, we present a photoionization study of C_2H_5I and C_6H_6 doped into Ar and SF_6. The dopant C_2H_5I was chosen because of the similarity of its electronic structure to that of CH_3I [14,15]. The dopant C_6H_6, on the other hand, was chosen because of the *lack* of any similarity to CH_3I. The perturber Ar was selected because of its small electron affinity, which makes this perturber a prime candidate for investigating pathway 2 [i.e., eqs. (3, 4)]. The perturber SF_6, on the other hand, was selected because of its large electron affinity, which makes this perturber a prime candidate for investigating pathway 1 [i.e., eqs. (1,2)]. As will be reported below, pure C_2H_5I and pure C_6H_6 (unlike pure CH_3I) do not exhibit subthreshold photocurrent, which indicates that pathway 2 should not be available in these systems. This inability to access pathway 2 is further substantiated here by the absence of subthreshold photoionization in C_2H_5I and C_6H_6 doped into Ar. However, both C_2H_5I and C_6H_6 doped into SF_6 exhibit rich subthreshold photoionization structure which will be modeled within the confines of pathway 1 [eqs. (1, 2 and 11)].

Finally, the origin of subthreshold photoionization structure in high-n Rydberg states has also permitted the determination of zero-kinetic-energy electron scattering lengths of highly absorbing perturbers [8,10,14]. This determination of electron scattering lengths from perturber-induced energy shifts of high-n Rydberg states follows from a theory by Fermi [22], as modified by Alekseev and Sobel'man [23]. Briefly, these authors [22,23] concluded that the total perturber-induced energy shift is a sum of two contributions,

$$\Delta = \Delta_{sc} + \Delta_p , \qquad (13)$$

where Δ_{sc} is the 'scattering' shift and Δ_p is the 'polarization' shift. The polarization shift Δ_p, which results from the interaction of the cationic core of the Rydberg molecule with the perturber molecule, is given by [2,23]

$$\Delta_p = - 10.78 \left(\frac{1}{2} \alpha e^2 \right)^{2/3} (\hbar v)^{1/3} \rho_P , \qquad (14)$$

where α is the polarizability of the perturber molecule, e is the charge of the electron, v is the relative thermal velocity of the molecules and $\hbar$ is the reduced Planck constant. Since Δ_p is easily calculated and Δ is determined from the experimental spectra, Δ_{sc} can be obtained from eq. (13). However, the scattering shift Δ_{sc}, which is due to the interaction between the quasi-free electron and the perturber medium, is given by [22]

$$\Delta_{sc} \equiv \left(\frac{2 \pi \hbar}{m} \right) A \rho_P , \qquad (15)$$

where m is the mass of the electron and A is the zero-kinetic-energy electron scattering length of the perturber. Therefore, the value for Δ_{sc} obtained from eq. (13) can be used to determine the zero-kinetic-energy electron scattering length A via eq. (15).

In the present Paper, since we can assign the subthreshold photoionization structure to high-n Rydberg states of the dopant, we have extracted the electron scattering length of SF_6 from the density-dependent energy shifts of the subthreshold structure of C_2H_5I and C_6H_6. The values obtained from the measurements presented here accord well with those values obtained from a similar analysis of the subthreshold photocurrent of CH_3I/SF_6 [14], as well as from the autoionization spectra of CH_3I/SF_6 [13]. Since Ar is transparent in the spectral region of interest, we were also able to obtain the electron scattering length of Ar from both the absorption spectra and the autoionization spectra of C_2H_5I doped into Ar. The value extracted from these measurements agrees nicely with that obtained from similar absorption studies of CH_3I [2,3] and C_6H_6 [5] in Ar, as well as with that obtained from field ionization measurements of CH_3I in dense Ar [16,24].

2. Experiment

The experimental apparatus has been described in detail previously [14,25]. Briefly, photoionization and photoabsorption spectra were measured using monochromatized synchrotron radiation having a resolution of 0.09 nm, or ~ 8 meV in the spectral region of interest. The copper experimental cell, which has a path length of 1.0 cm, was equipped with entrance and exit MgF_2 windows and a pair of parallel-plate electrodes (stainless steel, 3.0 mm spacing) oriented perpendicular to the windows. This arrangement of electrodes and windows allowed for the simultaneous recording of transmission and photoionization spectra. The cell, which is capable of withstanding pressures up to 100 bar, was connected to a cryostat and heater system allowing the temperature to be controlled to within ± 1 K. The applied electric field was 100 V, and all reported spectra are current saturated. (Current saturation was verified by measuring selected spectra at different electric field strengths. Photocurrents within the cell were of the order of 10^{-10} A.)

The intensity of the synchrotron radiation exiting the monochromator was monitored by measuring the photoemission current from a metallic grid intercepting the beam prior to the experimental cell. All photoionization spectra are normalized to this current. Transmission spectra (which are reported as absorption = 1 - transmission) are normalized both to the incident light intensity and to the empty cell transmission.

C_2H_5I (Sigma, 99%), C_6H_6 (Aldrich Chemical, 99.9+%), SF_6 (Matheson Gas Products, 99.996%) and Ar (Matheson Gas Products, 99.9999%) were used without further purification. The gas handling system has been described previously, as have the procedures employed to ensure a homogenous mixing of dopant and perturber [7].

3. Results and Discussion

In Fig. 1 and Fig. 2, we present subthreshold photoionization spectra of C_2H_5I and C_6H_6, respectively, doped into SF_6, in comparison to the low pressure photoabsorption spectra of the dopant. Over the same number density ranges as those given in Figs. 1 and 2, C_2H_5I and C_6H_6 doped into Ar exhibited no subthreshold photoionization structure. (All C_2H_5I spectra presented are normalized to unity at the same spectral feature above the $\tilde{X}_1\ ^2E_{1/2}$ [26,27] ionization threshold. All C_6H_6 spectra are normalized to unity at the same spectral feature above the $^2E_{1g}$ [28] ionization threshold.) Since the onset of the subthreshold photocurrent signal is far below the first ionization limit of the dopant at room temperature (0.27 eV below for C_2H_5I, 0.22 eV below for C_6H_6), the collisional transfer of translational, rotational or vibrational energy from the perturber to the dopant can be discounted as a possible

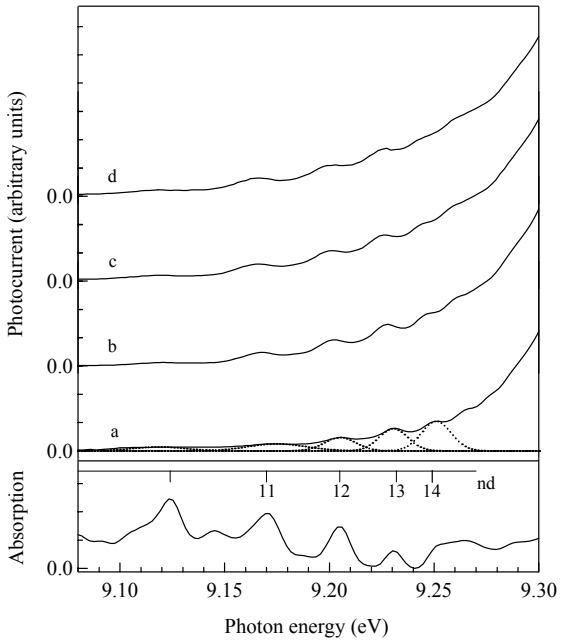

Fig. 1. Subthreshold photoionization spectra of C_2H_5I/SF_6 at 300 K. Absorption of pure C_2H_5I: 0.5 mbar. Photoionization of 0.1 mbar C_2H_5I in varying SF_6 number densities (10^{19} cm^{-3}): a, 0.12; b, 0.73; c, 1.5; d, 2.2. Each spectrum is normalized to unity at the same spectral feature above the $\tilde{X}_1\ ^2E_{1/2}$ ionization threshold. In (a), the dotted lines are an example of the gaussian fits used to obtain peak intensities.

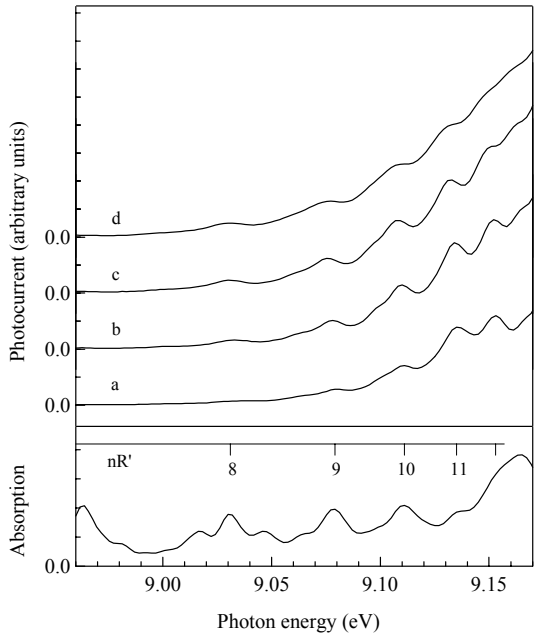

Fig. 2. Subthreshold photoionization spectra of C_6H_6/SF_6 at 300 K. Absorption of pure C_6H_6: 1.0 mbar. Photoionization of 1.0 mbar C_6H_6 in varying SF_6 number densities (10^{19} cm^{-3}): a, 0.12; b, 0.49; c, 1.1; d, 2.2. Each spectrum is normalized to unity at the same spectral feature above the $^2E_{1g}$ ionization threshold.

ionization mechanism leading to this structure. Furthermore, as was also the case for CH_3I/Ar [15] and CH_3I/SF_6 [14], we observed no temperature effect on the relative intensities of the subthreshold structure, thereby ruling out vibrational autoionization a possible mechanism. (The absence of any temperature dependence was verified by measuring subthreshold photoionization spectra for various dopant/perturber sample pressures at various temperatures (in the range -40°C to 80°C) for both systems. With the exception of a temperature dependent background (see below), no change was observed in these subthreshold spectra.) We also observed no subthreshold features in pure C_2H_5I (0.1 mbar - 160 mbar) and pure C_6H_6 (1 mbar - 100 mbar). Therefore, as discussed in the introduction, the most probable mechanisms leading to subthreshold photoionization are those of pathway 1 [i.e., eqs. (1, 2)].

We have obtained peak areas for the subthreshold photocurrent shown in Figs. 1 and 2 by integrating a gaussian deconvolution of various peaks. (An example of part of a gaussian deconvolution used to obtain the peak areas is shown in Fig. 1a.) The values for these peak areas are plotted in Fig. 3 versus the number density of SF_6, and are listed in Table 1 (C_2H_5I /SF_6) and Table 2 (C_6H_6/SF_6). Clearly, the intensity of the subthreshold photoionization is linearly dependent on the perturber number density, which is in accord with pathway 1 [cf. eq. (11)]. Since the subthreshold structure is superimposed on a rising exponential background (as discussed by Ivanov and Vilesov [11,12]), we have also subtracted an exponential background fitted to the zero baseline and the photocurrent step at

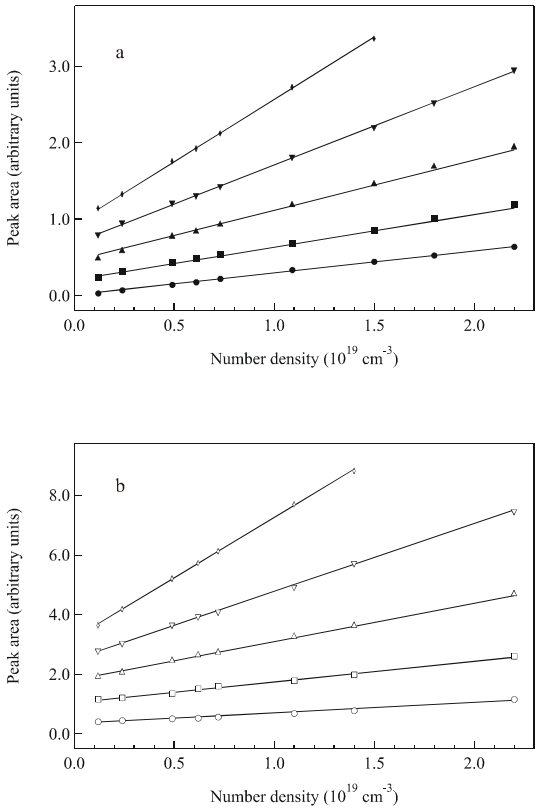

Fig. 3. Peak areas (by gaussian fits to the photoionization spectra) for the subthreshold photoionization structure of (a) 0.1 mbar C_2H_5I and (b) 1.0 mbar C_6H_6 as a function of SF_6 number density. In (a): ●, 10d; ■, 11d; ▲, 12d; ▼, 13d; ◆, 14d. In (b): ○, 8R'; □, 9R'; △, 10R'; ▽, 11R'; ◇, 12R'. The solid lines represent a least-squares fit to the function $b_0 + b_1 \rho$.

Table 1. Peak areas (by gaussian fits to the photoionization spectra) for the subthreshold photoionization structure (cf. Fig. 3) of 0.1 mbar C_2H_5I in varying SF_6 number densities ρ (10^{19} cm^{-3})

ρ	10d	11d	12d	13d	14d
0.12	0.0301	0.242	0.497	0.785	1.14
0.24	0.0710	0.318	0.594	0.940	1.33
0.49	0.142	0.433	0.784	1.20	1.76
0.61	0.176	0.483	0.848	1.30	1.92
0.73	0.221	0.543	0.941	1.42	2.12
1.09	0.336	0.683	1.20	1.80	2.73
1.5	0.445	0.856	1.47	2.19	3.36
1.8	0.526	1.02	1.70	2.51	
2.2	0.640	1.19	1.95	2.94	
Regression Coefficients[*]					
b_0	0.0118	0.207	0.458	0.686	0.935
b_1	0.286	0.427	0.659	1.02	1.63

[*]The regression coefficients are for a least-squares linear fit, $b_0 + b_1 \rho_0$, as shown in Fig. 5a.

threshold. The resulting spectra, when analyzed for peak areas, yields plots similar in detail to the ones shown in Fig. 3.

Table 2. Peak areas (by gaussian fits to the photoionization spectra) for the subthreshold photoionization structure (cf. Fig. 4) of 1.0 mbar C_6H_6 in varying SF_6 number densities ρ (10^{19} cm^{-3})

ρ	8R'	9R'	10R'	11R'	12R'
0.12	0.407	1.16	1.95	2.75	3.63
0.24	0.443	1.22	2.09	3.00	4.17
0.49	0.508	1.36	2.48	3.62	5.20
0.62	0.529	1.52	2.67	3.90	5.71
0.72	0.565	1.60	2.76	4.05	6.11
1.1	0.687	1.79	3.29	4.89	7.69
1.4	0.778	1.98	3.65	5.68	8.81
2.2	1.15	2.60	4.72	7.42	
Regression coefficients[*]					
b_0	0.356	1.05	1.81	2.50	3.21
b_1	0.351	0.690	1.29	2.28	4.05

[*]The regression coefficients are for a least-squares linear fit, $b_0 + b_1 \rho$, as shown in Fig. 5b.

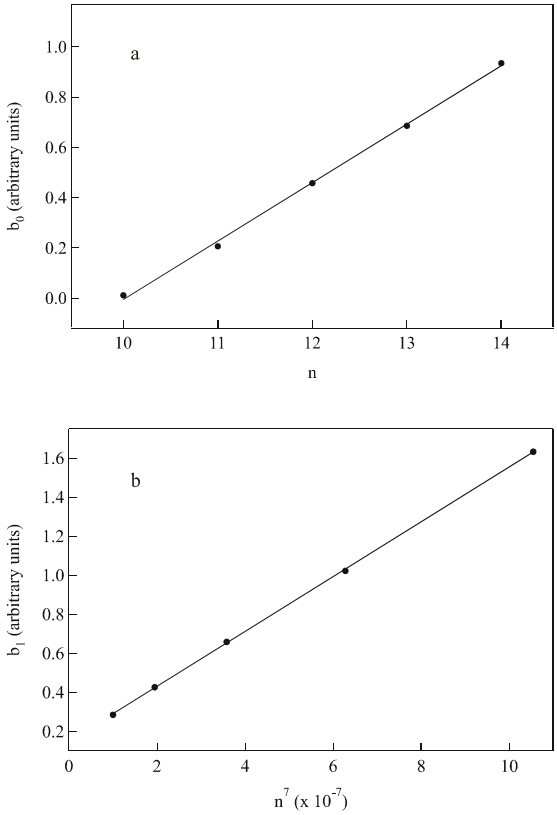

Fig. 4. (a) Constant and (b) linear regression coefficients for the subthreshold density dependence of C_2H_5I/SF_6 (Table 2) plotted versus the C_2H_5I excited state principal quantum number n and n^7, respectively. The straight lines are least-squares fits to the data. See text for discussion.

The linear plots of Fig. 3 are in accord with pathway 1 [i.e., eqs. (1,2, and 11)] for ρ_D = constant, and may be expressed as

$$i = b_0 + b_1 \rho_P . \qquad (16)$$

The linear correlation coefficients b_0 (= $k_1 \rho_D$) and b_1 (= $k_2 \rho_D$) are given in Table 1 (C_2H_5I/SF_6) and Table 2 (C_6H_6/SF_6). Since the linear correlation coefficients b_0 and b_1 are proportional to k_1 and k_2, respectively, b_0 and b_1 should have the same n dependence as k_1 and k_2. In Fig. 4 (C_2H_5I/SF_6) and Fig. 5 (C_6H_6/SF_6), we have plotted b_0 versus n and b_1 versus n^7. The linearity of these figures, when coupled with the analysis of Fig. 3, allows one to conclude that pathway 1 [i.e., eqs. (1, 2 and 11)] is sufficient to explain the behavior of the subthreshold photoionization in both C_2H_5I/SF_6 and C_6H_6/SF_6. (However, as mentioned in the

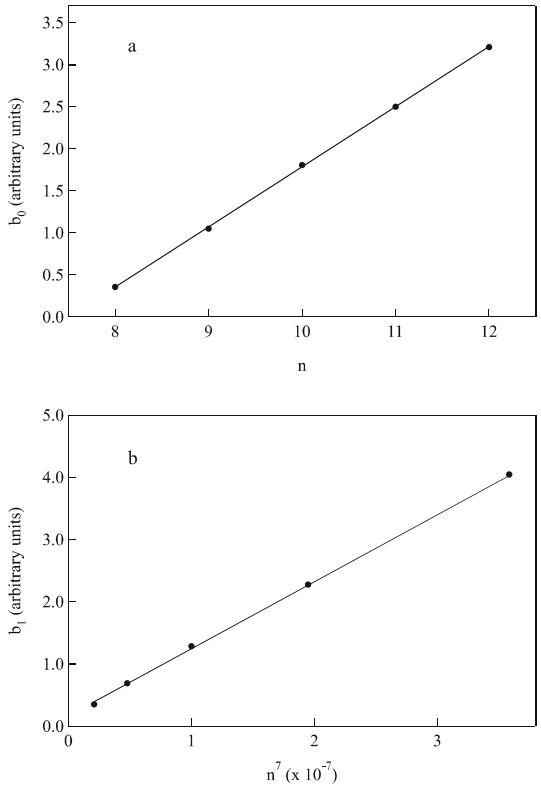

Fig. 5. (a) Constant and (b) linear regression coefficients for the subthreshold density dependence of C_6H_6/SF_6 (Table 3) plotted versus the C_6H_6 excited state principal quantum number n and n^7, respectively. The straight lines are least-squares fits to the data. See text for discussion.

introduction, other mechanisms are possible so long as these mechanisms scale as n (and are saturated) or as n^7.) Unlike the case of CH_3I, which exhibits subthreshold photoionization structure in pure CH_3I [14], CH_3I/Ar [15] and CH_3I/SF_6 [14], the dopants C_2H_5I and C_6H_6 appear to exhibit subthreshold photoionization in C_2H_5I/SF_6 and C_6H_6/SF_6 arising only from pathway 1 [i.e., eqs. (1, 2, and 11)] in the absence of pathway 2 [i.e., eqs. (3, 4 and 12)].

Since we can assign the subthreshold photoionization structure to high-n Rydberg states of the dopant, we have used the density-dependent energy shifts of this structure to obtain the zero-kinetic-energy electron scattering length of SF_6. In Table 3, the energy positions of a number of C_2H_5I nd Rydberg states [26,27], as assigned from the

Table 3. nd and $I_1 \equiv I(\tilde{X}_1\ ^2E_{1/2})$ photoionization energies (eV) of C_2H_5I in selected number densities ρ (10^{19} cm^{-3}) of SF_6.

ρ	10d	11d	12d	13d	14d	I_1
0.12	9.122	9.171	9.203	9.228	9.249	9.349
0.49	9.120	9.169	9.203	9.227	9.249	9.348
0.73	9.119	9.167	9.201	9.226	9.248	9.347
1.5	9.117	9.166	9.200	9.225	9.246	9.346
2.2	9.116	9.165	9.198	9.223		9.343

photoionization spectra, are given for selected SF_6 number densities. Ionization energies I_1 [$\equiv I(\tilde{X}_1\ ^2E_{1/2})$] extracted from a fit of the assigned spectra to the Rydberg equation are also given in Table 3. The energy positions of a number of C_6H_6 nR' states [27,28], as well as the values of I_1 [$\equiv I(^2E_{1g})$] extracted from a fit of the assigned spectra to the Rydberg equation, are presented in Table 4 for selected SF_6 number densities. The shift data are summarized in Figs. 6a and 6b, where we have plotted the energy positions of nd C_2H_5I and nR' C_6H_6 Rybderg states, respectively, versus SF_6 number density. Fig. 6 shows that the energy shifts are linearly dependent on the perturber number density and can therefore be analyzed by the Fermi model given in eqs. (13-15) of the introduction. Using the value [29] $\alpha = 6.54 \times 10^{-24}$ cm^3 for SF_6, and the value $\Delta/\rho = -25.36 \times 10^{-23}$ eV cm^3 obtained from the subthreshold photoionization spectra of C_2H_5I doped into SF_6, one finds a zero-

Table 4. nR' and $I_1 \equiv I(^2E_{1g})$ photoionization energies (eV) of C_6H_6 in selected number densities ρ (10^{19} cm^{-3}) of SF_6.

ρ	8R'	9R'	10R'	11R'	12R'	I_1
0.12	9.030	9.079	9.110	9.134	9.153	9.244
0.24	9.029	9.078	9.110	9.134	9.153	9.243
0.49	9.028	9.077	9.109	9.133	9.152	9.242
0.72	9.027	9.076	9.108	9.132	9.151	9.241
1.1	9.027	9.075	9.107	9.131	9.150	9.240
2.2	9.025	9.074	9.106	9.130		9.239

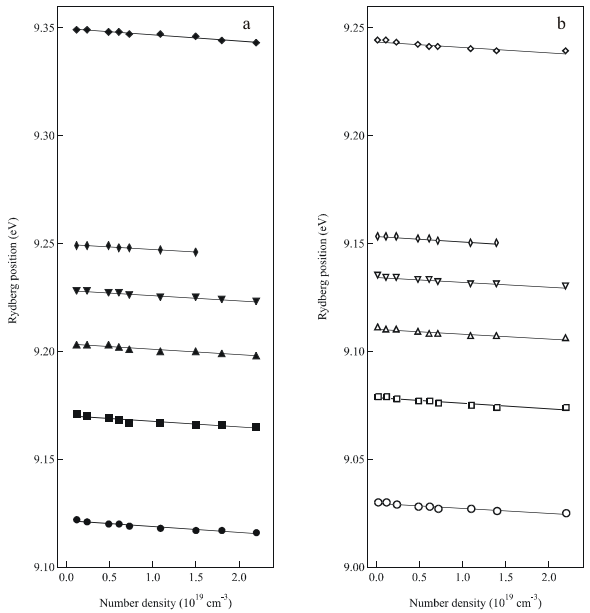

Fig. 6. Energy shifts of (a) nd Rydberg states of C_2H_5I and (b) the nR' Rydberg states of C_6H_6 as a function of SF_6 number density ρ (10^{19} cm^{-3}). In (a): ●, 10d; ■, 11d; ▲, 12d; ▼, 13d; ♦, 14d; ◆, I_1 ($\tilde{X}_1\,^2E_{1/2}$). In (b): ○, 8R'; □, 9R'; △, 10R'; ▽, 11R'; ♢, 12R'; ◇, I_1 ($^2E_{1g}$) The solid lines represent a least-squares linear fit.

kinetic-energy electron scattering length of A = -0.497 nm for SF_6. Similarly, the value Δ/ρ = -24.21 x 10^{-23} eV cm^3 obtained from C_6H_6/SF_6 yields a zero-kinetic-energy electron scattering length of A = -0.473 nm. Both scattering lengths obtained in the present study accord well with the scattering length A = -0.492 nm determined by an analysis of the subthreshold structure of CH_3I/SF_6 [14], and A = -0.484 nm determined from the perturber-induced energy shift of CH_3I autoionization spectra [13].

Since Ar is transparent in the region of the first ($I_1 \equiv I(\tilde{X}_1\,^2E_{1/2})$ = 9.349 eV [27,28]) and second ($I_1 \equiv I(\tilde{X}_2\,^2E_{1/2})$ = 9.932 eV [27,28]) ionization energies of C_2H_5I, we were also able to obtain the perturber-induced energy shifts of C_2H_5I doped into Ar from both the autoionization spectra and the photoabsorption spectra of C_2H_5I/Ar. These data allowed us to determine the zero-kinetic-energy electron scattering length of Ar. In Fig. 7, we present photoabsorption spectra of C_2H_5I doped into varying number densities of Ar. (The autoionization spectra for C_2H_5I/Ar reproduce the photoabsorption structure in the autoionizing region and, for that reason, are not presented here.) The energy shifts obtained from the photoabsorption measurements are summarized in Table 5 and plotted in Fig. 8. (The energy shifts obtained from the autoionization spectra are identical (to within experimental error) to the energy shifts presented in Table 5.) Using the perturber induced energy shifts of C_2H_5I in Ar extracted from the photoabsorption spectra, and using eqs. (13) - (15) with the value [30] α = 1.66 x 10^{-24} cm^3, we obtain an electron scattering length for Ar of A = - 0.086 nm. This value agrees well with A = - 0.089 nm obtained from similar measurements involving CH_3I [2,3] and C_6H_6 [5] doped into Ar, and A = -0.082 nm obtained from field ionization measurements of

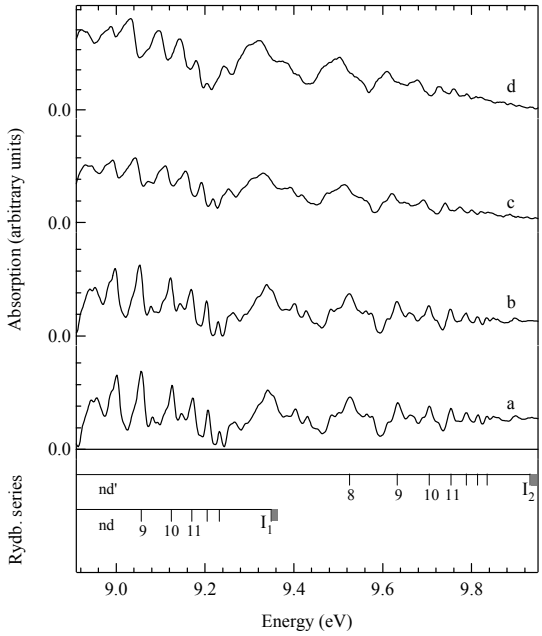

Fig. 7. Photoabsorption spectra of C_2H_5I/Ar at 300 K. Photoabsorption spectra of (a) 0.5 mbar C_2H_5I and C_2H_5I doped into varying number densities of Ar (10^{20} cm^{-3}): b, 0.024; c, 2.38; d, 4.87. The concentration of C_2H_5I was kept below 10 ppm in Ar. All absorption spectra are corrected for the empty cell transmission. The assignment given at the bottom corresponds to the pure C_2H_5I spectrum.

Table 5. nd and $I_1 \equiv I(\tilde{X}_1\ ^2E_{1/2})$ as well as nd' and $I_2 \equiv I(\tilde{X}_2\ ^2E_{1/2})$ photoabsorption energies (eV) of C_2H_5I in selected number densities ρ (10^{20} cm^{-3}) of Ar.

nd and $I_1 \equiv I(\tilde{X}_1\ ^2E_{1/2})$

ρ	10d	11d	12d	13d	I_1
0.024	9.123	9.169	9.204	9.231	9.348
0.13	9.122	9.168	9.203	9.230	9.347
0.24	9.121	9.167	9.203	9.229	9.346
0.66	9.120	9.165	9.201	9.227	9.345
1.24	9.117	9.163	9.199	9.223	9.340
2.38	9.110	9.158	9.194	9.218	9.336
3.75	9.104	9.149	9.186	9.215	9.329
4.87	9.100	9.146	9.183	9.207	9.324

nd' and $I_2 \equiv I(\tilde{X}_2\ ^2E_{1/2})$

ρ	10d'	11d'	12d'	13d'	14d'	I_2
0.0243	9.704	9.753	9.787	9.813	9.834	9.931
0.13	9.704	9.752	9.786	9.812	9.833	9.930
0.24	9.703	9.751	9.785	9.811	9.832	9.929
0.66	9.701	9.750	9.784	9.810	9.831	9.928
1.24	9.697	9.747	9.780	9.806	9.828	9.923
2.38	9.691	9.741	9.775	9.801	9.823	9.918
3.75	9.684	9.736	9.769	9.794		9.912
4.87	9.677	9.729	9.763	9.789		9.909

CH_3I doped into dense Ar [16,24].

In summary, we have measured photoionization and photoabsorption spectra of C_2H_5I/Ar and C_6H_6/Ar and photoionization spectra of C_2H_5I/SF_6 and C_6H_6/SF_6, as a function of the perturber number density. We have shown that pathway 1 [i.e., eqs. (1, 2 and 11)], which depends upon direct dopant/perturber interactions, is sufficient to explain the origin of subthreshold photoionization in both C_2H_5I and C_6H_6 doped into SF_6. We have also shown that pathway 2 [i.e., eqs. (3, 4 and 12)] is likely unavailable as a subthreshold photoionization mechanism in both C_2H_5I and C_6H_6, since subthreshold photoionization is absent in pure C_2H_5I, pure C_6H_6, C_2H_5I/Ar and C_6H_6/Ar. (The inaccessibility of pathway 2 may be due, in part, to the inability of C_2H_5I and C_6H_6 to form stable dimers in a static system. However, resolving this issue completely will require a detailed mass analysis (as originally discussed by Ivanov and Vilesov [11] for CH_3I) in a molecular beam experiment.) We have shown that the correlation coefficients b_0 and b_1 scale in a simple fashion according to the principal quantum number of the dopant Rydberg state, which allows us to conclude that the mechanisms of electron attachment to SF_6, and associative ionization with SF_6, are sufficient to explain the behavior of the subthreshold photocurrent. Additional measurements where the *perturber* number density is held constant while the *dopant* number density is varied will provide a further test of the applicability of pathway 1 [i.e., eqs. (1, 2 and 11)] and pathway 2 [i.e., eqs. (3, 4 and 12)] for general dopant/perturber systems. (These measurements are currently in progress by us for CH_3I/Ar and CH_3I/SF_6 [31], for example.)

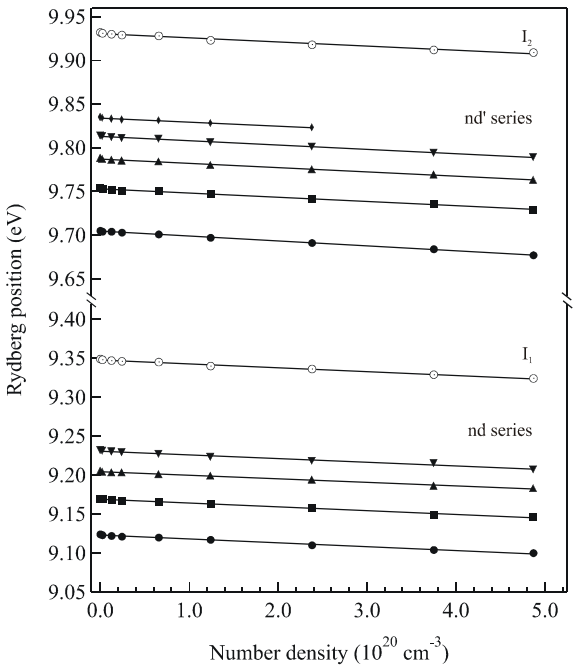

Fig. 8. Energy shifts of nd and nd' Rydberg states of C_2H_5I as a function of Ar number density ρ (10^{20} cm^{-3}). ●, n = 10; ■, n = 11; ▲, n = 12; ▼, n = 13; ◆, n = 14. The fitted ionization energies are also shown. All straight lines are least-squares fits.

Finally, we have used the density-dependent energy shifts of high-n Rydberg states, extracted from the subthreshold photoionization spectra of C_2H_5I and C_6H_6 doped into SF_6, to determine the zero-kinetic-energy scattering length of SF_6. The values obtained from these measurements were shown to agree with that obtained by similar measurements of CH_3I/SF_6 [13,14]. We also presented photoabsorption spectra of C_2H_5I doped into Ar and used these spectra to obtain the zero-kinetic-energy electron scattering length of Ar. This value was shown to accord both with the scattering lengths obtained from photoabsorption measurements of CH_3I/Ar [2,3] and C_6H_6/Ar [5], as well as with the value extracted from field ionization measurements of CH_3I doped into dense Ar [16,24].

Acknowledgments

This work was carried out at the University of Wisconsin Synchrotron Radiation Center (NSF DMR95-31009) and was supported by a grant from the Louisiana Board of Regents Support Fund (LEQSF (1997-00)-RD-A-14).

References

1. M. B. Robin, *Higher Excited States of Polyatomic Molecules, Vol. III* (Academic Press, Orlando, 1985).
2. A. M. Köhler, Ph.D. Dissertation, University of Hamburg, Hamburg, 1987.
3. A. M. Köhler, R. Reininger, V. Saile, G. L. Findley, Phys. Rev. A **35**, 79 (1987).
4. U. Asaf, W. S. Felps, K. Rupnik, S. P. McGlynn, and G. Ascarelli, J. Chem. Phys. **91**, 5170 (1989).
5. R. Reininger, E. Morikawa and V. Saile, Chem. Phys. Lett. **159**, 276 (1989).
6. T. F. Gallagher, *Rydberg Atoms* (Cambridge Univ. Press, Cambridge, 1994).
7. J. Meyer, R. Reininger, U. Asaf and I. T. Steinberger, J. Chem. Phys. **94**, 1820 (1991)
8. U. Asaf, I. T. Steinberger, J. Meyer and R. Reininger, J. Chem. Phys. **95**, 4070 (1991).
9. U. Asaf, J. Meyer, R. Reininger, and I. T. Steinberger, J. Chem. Phys. **96**, 7885 (1992).
10. I. T. Steinberger, U. Asaf, G. Ascarelli, R. Reininger, G. Reisfeld and M. Reshotko, Phys. Rev. A **42**, 3135 (1990).
11. V. S. Ivanov and F. I. Vilesov, Opt. Spectrosc. **36**, 602 (1974) [Opt. Spektrosk. **36**, 1023 (1974)].
12. V. S. Ivanov and F. I. Vilesov, Opt. Spectrosc. **39**, 487 (1975) [Opt. Spektrosk **39**, 857 (1975)].
13. C. M. Evans, R. Reininger, and G. L. Findley, Chem. Phys. Lett. **297**, 127 (1998).
14. C. M. Evans, R. Reininger, and G. L. Findley, Chem. Phys. **241**, 239 (1999).
15. C. M. Evans, R. Reininger and G. L. Findley, Chem. Phys. Lett., **322**, 465 (2000).
16. A. K. Al-Omari, Ph.D. Dissertation, University of Wisconsin-Madison, Wisconsin, 1996.
17. J. Meyer, U. Asaf and R. Reininger, Phys. Rev. A **46**, 1673 (1992)
18. A. Rosa and I. Szamrej, J. Phys. Chem. A **104**, 67 (2000).
19. J. O. Hirschfelder, C. F. Curtiss and R. B. Bird, *Molecular Theory of Gases and Liquids* (John Wiley, New York, 1964).
20. A. V. Phelps and R. J. Van Brunt, J. Appl. Phys. **64**, 4269 (1988).
21. J. H. D. Eland and J. Berkowitz, J. Chem. Phys. **67**, 5034 (1977).
22. E. Fermi, Nuovo Cimento **11**, 157 (1934).
23. V. A. Alekseev and I. I. Sobel'man, Sov. Phys. JETP **22**, 882 (1966).
24. J. Meyer, R. Reininger and U. Asaf, Chem. Phys. Lett. **173**, 384 (1990).
25. A. K. Al-Omari and R. Reininger, J. Chem. Phys. **103**, 506 (1995).
26. N. Knoblauch, A. Strobel, I. Fischer and V. E. Bondybey, J. Chem. Phys. **103**, 5417 (1995).
27. G. Herzberg, *Electronic Spectra and Electronic Structure of Polyatomic Molecules* (Krieger, Malabar, FL, 1991).
28. R. G. Neuhauser, K. Siglow and H. J. Neusser, J. Chem. Phys. **106**, 896 (1997).
29. R. D. Nelson and R. H. Cole, J. Chem. Phys. **54**, 4033 (1971).
30. R. H. Orcutt and R. H. Cole, J. Chem. Phys. **46**, 697 (1967).
31. C. M. Evans and G. L. Findley, Chem. Phys., to be submitted.